The Stress-response protein prostate-associated gene 4, interacts with c-Jun and potentiates its transactivation

CrossMark

Krithika Rajagopalan [a,1,2], Ruoyi Qiu [d,1], Steven M. Mooney [a], Shweta Rao [a], Takumi Shiraishi [a], Elizabeth Sacho [d], Hongying Huang [c], Ellen Shapiro [c], Keith R. Weninger [d,*], Prakash Kulkarni [a,b,**]

[a] Department of Urology, Johns Hopkins University School of Medicine, Baltimore, MD 21287, USA
[b] Oncology, Johns Hopkins University School of Medicine, Baltimore, MD 21287, USA
[c] Department of Urology, New York University School of Medicine, New York, NY 10016, USA
[d] Department of Physics, North Carolina State University, Raleigh, NC 27695, USA

ARTICLE INFO

ABSTRACT

The Cancer/Testis Antigen (CTA), Prostate-associated Gene 4 (PAGE4), is a stress-response protein that is upregulated in prostate cancer (PCa) especially in precursor lesions that result from inflammatory stress. In cells under stress, translocation of PAGE4 to mitochondria increases while production of reactive oxygen species decreases. Furthermore, PAGE4 is also upregulated in human fetal prostate, underscoring its potential role in development. However, the proteins that interact with PAGE4 and the mechanisms underlying its pleiotropic functions in prostatic development and disease remain unknown. Here, we identified c-Jun as a PAGE4 interacting partner. We show that both PAGE4 and c-Jun are overexpressed in the human fetal prostate; and in cell-based assays, PAGE4 robustly potentiates c-Jun transactivation. Single-molecule Förster resonance energy transfer experiments indicate that upon binding to c-Jun, PAGE4 undergoes conformational changes. However, no interaction is observed in presence of BSA or unilamellar vesicles containing the mitochondrial inner membrane diphosphatidylglycerol lipid marker cardiolipin. Together, our data indicate that PAGE4 specifically interacts with c-Jun and that, conformational dynamics may account for its observed pleiotropic functions. To our knowledge, this is the first report demonstrating crosstalk between a CTA and a proto-oncogene. Disrupting PAGE4/c-Jun interactions using small molecules may represent a novel therapeutic strategy for PCa.

© 2013 Elsevier B.V. All rights reserved.

1. Introduction

Prostate-associated gene 4 (PAGE4) is a member of the Cancer/Testis Antigen (CTA) family of genes that is typically expressed in testicular germ cells, is silent in most somatic tissues, but is aberrantly expressed in several types of cancer [1–3] including prostate cancer (PCa) [4]. PAGE4 is also a developmentally-regulated gene that is upregulated in the fetal prostate compared to the normal adult gland. Further, in addition to frank prostate adenocarcinoma lesions, PAGE4 expression is highly upregulated in proliferative inflammatory atrophy (PIA) (Zeng et al., unpublished) and high-grade prostatic intraepithelial neoplasia (HG-PIN) lesions [5]. Both PIA and HG-PIN are thought to result from inflammatory stress and represent tumorigenic precursors [6]. Hence, the dramatic upregulation of PAGE4 in these precursor lesions strongly suggests that PAGE4 may be a stress-response protein.

Consistent with a stress-response function, PAGE4 protein levels are upregulated when PCa cells are treated with various stress factors including the proinflammatory cytokine TNFα. In cells challenged with stress, there is increased translocation of the PAGE4 protein to the mitochondrion and suppressed reactive oxygen species production. Furthermore, p21 is elevated in a p53-independent manner in PAGE4 overexpressing cells which results in impeded cell cycle progression, attenuated stress-induced DNA damage, and decreased cell death (Zeng et al., unpublished). Thus, overexpression of PAGE4 in the stress-enriched PCa microenvironment appears to be a protective response to

reduce cellular damage while contributing to PCa development. However, the mechanism(s) underlying these pleiotropic functions of PAGE4 in prostatic development and disease are not fully understood and the proteins that interact with it remain unidentified.

One clue to its potential function became apparent when we discovered that PAGE4, like the majority of the CTAs, is a highly intrinsically disordered protein (IDP) [7,8]. In contrast to the prevailing notion that proteins are highly structured molecules and that structure defines function, research over the last 15 years has revealed that a significant fraction of the proteome of organisms across all living kingdoms is unstructured or intrinsically disordered [9]. Thus, IDPs are proteins that, under physiological conditions, at least in vitro, lack rigid 3D structures either along their entire length or in localized regions of the molecule. Despite the lack of structure, IDPs play important biological roles that include transcriptional regulation and signaling via protein–protein interaction networks [10,11].

A comprehensive study of protein interaction networks (PINs) from yeast to humans revealed that proteins that constitute hubs in a PIN are significantly more disordered compared to proteins that constitute edges [12,13], underscoring the role of IDPs in signaling. Consistent with the preference for IDPs to occupy hub positions, most IDPs rapidly undergo disorder-to-order transitions upon binding to their biological target (coupled folding and binding) in order to perform their function [14]. Thus, conformational dynamics is believed to represent a major functional advantage for the IDPs, enabling them to interact with a broad range of biological targets under normal physiological conditions where their expression is tightly regulated [15,16]. However, experimental evidence demonstrating conformational dynamics in IDPs is limited to only a few examples [17–25].

Intrinsic disorder also appears to be an important determinant of dosage-sensitive effects. Thus, IDPs are prone to initiate promiscuous interactions when overexpressed, suggesting that this is the likely cause of the resulting toxicity/pathology. Indeed, studies in model organisms provide compelling evidence supporting this causality [26]. Interestingly, the same properties are strongly associated with dosage-sensitive oncogenes as well as several other cancer-associated genes [27] suggesting that mass action driven molecular interactions may be a frequent cause of cancer [26,28]. In fact, numerous IDPs are also associated with several other human diseases [11], underscoring the link between intrinsic protein disorder, promiscuity, and dosage sensitivity.

The structural flexibility of IDPs could also contribute significantly to 'noise' in the PINs especially when IDP expression is dysregulated. Indeed, recent evidence indicates that the information transduced in cellular signaling pathways is significantly affected by noise [29,30]. In fact, it has been proposed that noise in these pathways is generated by the interconnected and promiscuous nature of the PINs and that this source of noise significantly influences the way signals are transmitted. Therefore, noise may be considered an integral part of the correct transmission of signals and signaling cascades including those that play a role in the fidelity of epigenetic memory [31]. We recently hypothesized that noise due to IDP conformational dynamics can rewire PINs to cause phenotypic switching such as the transformation of a normal cell to a cancer cell [32]. Because noise affects central regulatory switches in cell functions, it is plausible that alterations in noise level could induce pathological states such as cancer [31]. It is therefore imperative to identify proteins that interact with PAGE4.

In this work, we serendipitously identified the proto-oncogene c-Jun as a PAGE4 interacting partner. Employing a cell-based reporter system we demonstrate that PAGE4 interacts with c-Jun and dramatically potentiates its transactivation. Furthermore, using single-molecule Förster resonance energy transfer (smFRET) microscopy, we show that PAGE4 changes conformations upon binding to c-Jun. Taken together, our results suggest that conformational dynamics may underlie the observed pleiotropic functions of PAGE4 during prostatic development and disease.

2. Materials and methods

2.1. Yeast two-hybrid screen

Matchmaker Gold yeast two-hybrid screening was performed according to manufacturer's instruction. Briefly, the cDNA encoding PAGE4 was inserted in frame into the multiple cloning sites of the DNA-BD vector, pGBKT7 (Clontech, Mountain View, CA), to generate the bait plasmid pGBKT7-PAGE4, which was subsequently confirmed by sequencing. The pGBKT7-PAGE4 plasmid was transformed into the bait strain Y2HGold. PAGE4 bait strain Y2HGold was mated with the pre-transformed Y187/pACT2 normalized universal human Mate & Plate cDNA library according to the Clontech protocol. Diploid yeast cells were plated on a nutrient deficiency medium SD double dropout plate without Trp and Leu (DDO) and analyzed for their ability to grow in the presence of highly toxic drug Aureobasidin A (125 ng/ml, Clontech) and regulate α-galactosidase expression, which hydrolyzes 5-bromo-4-chloro-3-indolyl-a-D-galactopyranoside (X-α-gal, 40 μg/ml, Clontech, Mountain View, CA) to produce a blue-end product. The selected colonies were restreaked on SD quadruple dropout plate without Trp, Leu, His and Ade (QDO) containing Aureobasidin A and X-α-gal for further selection.

2.2. DNA expression plasmid constructs

6His-PAGE4 was constructed by cloning the PCR product into pET28a as in [8]. A18C and P102C 6His-PAGE4 was created in pET28A via a QuikChange® Site-Directed Mutagenesis Kit (Stratagene, La Jolla, CA) using 6His-PAGE4 as a template. Cysteine residues were introduced at the 18th and 102nd position of PAGE4 using the following primers:

A18C_F:GAGGAAGAGGAGATGGTCAGGAGTGTCCCGATGTGGTTGCAT TCGTGG C
A18C_R:GCCACGAATGCAACCACATCGGGACAC TCCTGACCATCTCCT CTTCCTC
P102C_F:GACTAAAGAAGCAGGAGATGGGCAGTGCTAAAAGGGTGGGC GCGCCGACCC
P102C_R:GGGTCGGCGCGCCCACCCTTTTAGCACTGCCCATCTCCTGCTTC TTTAGTC.

nV5-PAGE4 was amplified from 6His-PAGE4 and cloned into the pcDNA™3.1/nV5-DEST (Invitrogen, Life technologies, Frederick, MD) according to the manufacturer's instructions. 6myc-ZNF394: ZNF394 cDNA was amplified from pCMV6-entry-ZNF394 (Origene, Rockville, MD) using gene specific primers containing BglII and XhoI sites. It was cloned into pcS3 + 6myc [33] with an N terminal 6myc tag.

2.3. Recombinant protein purification

WT/A18C/P102C PAGE4 and c-Jun were cloned into pet28A and subsequently transformed into BL21DE3pLySs (Invitrogen, Life technologies, Frederick, MD). Cells were induced with 0.5 mM isopropyl 1-thio-β-D-galactopyranoside (IPTG) for 3 h at 37 °C [34,35]. Recombinant protein was purified using the ProBond™ Purification System (Invitrogen, Life technologies, Frederick, MD) for purifying His-tagged proteins using a Nickel-NTA column. Bacterial cell lysates were prepared using denaturing conditions (6 M guanidine hydrochloride) and protein was purified using hybrid conditions (washing the column with denaturing buffer and subsequently washing with native wash buffer containing 20 mM imidazole). Eluted protein was concentrated using polyvinyl pyrollidone (PVP) and dialyzed against 1X Phosphate Buffered Saline (PBS).

2.4. Fluorescent dye labeling

Protein concentration was estimated using the BCA Protein Assay Reagent [36] (Thermo Scientific, Rockford, IL) and 0.5 M Pierce bond-breaker TCEP solution (Thermo Scientific, Rockford, IL) was added in a $10\times$ concentration over free cysteines. Dye labeling with either or both, Alexa Fluor® 555 and Alexa Fluor® 647 (Invitrogen, Life technologies, Frederick, MD) was carried out by resuspending dyes in 3 µl of DMSO. Samples were incubated with dye-DMSO for 10 min at room temperature followed by overnight incubation at 4 °C. The free dye was further separated from labeled protein using dialysis against 1X PBS followed by desalting using a Sephadex G50 column (Sigma Aldrich, St. Louis, MO).

2.5. Ensemble fluorescence characterization

Ensemble fluorescence anisotropy was measured with a QuantaMaster 40 spectrofluorometer (Photon Technology International, Birmingham, NJ). Alexa555 labeled PAGE4 was measured at 0.5 µM concentration alone or with 0.04 µg/µl concentration of c-Jun added to the cuvette. Fluorescence was excited at 532 nm and 5 emission scans from 550 nm to 600 nm were averaged. The peak emission integrated between 550 nm and 580 nm was used along with instrumental G factor corrections to calculate anisotropy values reported in the text [37]. The emission intensities in each of the channels of the QuantaMaster 40 spectrofluorometer were compared to calculate the ratio of quantum yield of Alexa555 conjugated to PAGE4 at 0.5 µM in the presence and absence of c-Jun, as described in the text.

2.6. Single molecule FRET studies

Proteins were immobilized on surfaces of custom made flow cells by direct immobilization or liposome encapsulation as described in the text and in further detail elsewhere [38,39]. Encapsulation used 100 nm diameter liposomes formed from egg phosphatidylcholine (PC) lipids doped with 0.1% biotinylated phosphatidylethanolamine (PE) lipids (both from Avanti Polar Lipids). Fluorescence intensities in donor and acceptor spectral bands were recorded from immobilized single molecules using a prism-type, total internal reflection single molecule FRET microscope equipped with a Dualview imager (Photometrics) that has been previously described [40]. The emCCD recorded frames at 10 Hz, and FRET efficiency were calculated from the intensities as $E = Ia/(Ia + Id)$. $\gamma = 1$ was used as a global correction [41] because analysis of γ from individual molecules with acceptor photobleaching accompanied with donor recovery yielded gamma values of 0.96, 0.92, and 0.99 for the A18C/63C mutant as well as 1.13, 1.01, 0.99 for the P102C/63C where the set of 3 numbers for each mutant reports experiments using PAGE4 with (in order) 1) no addition, 2) full-length c-Jun, or 3) truncated c-jun. FRET values in the text are reported as the center value and width of Gaussian fits to histograms assembled by accumulating all data points from molecules during FRET emitting intervals with active donor and acceptor dyes for greater than 500 molecules in each experiment. Supplementary Table 1 includes the values of the centers and widths of Gaussian fittings for all histograms in this work. We found that all histograms in this work could be fitted with single Gaussian functions that had widths consistent with expectations for the signal to noise ratios of our experiments [38,42] except those that included full length or truncated c-Jun. For those experiments, good fits were obtained using sums of two Gaussians where the center and width of one Gaussian was fixed those observed in the PAGE4 alone measurements. For double Gaussian fits, the fraction of events in each of the Gaussian peaks ranged from 30% to 70% and is listed in detail in Supplementary Table 1. Changes in peak center greater than 1/4 of the width were deemed as indicating distinct conformational state because control experiments indicated that experimental variation of histograms of identical samples is below

this level. All experiments were in buffer containing 20 mM Tris, 100 mM NaOAc, 5 mM $MgCl_2$ at pH 7.8.

2.7. Luciferase reporter assays

PC3 cells were seeded in a 24 well plate at approximately 20,000 cells/well. Cells were transiently transfected using X-tremeGENE HP DNA Transfection Reagent (Roche Diagnostics, Indianapolis, IN). The PathDetect Trans-reporting System (Agilent Technologies, Santa Clara, CA) was used to test the effect of PAGE4 on c-Jun transactivation using the manufacturer's instructions. Briefly, reporter plasmid pFR-Luc (250 ng) was co-transfected with pFA2-c-Jun transactivation plasmid (12.5 ng) or empty vector pFC2-DBD (12.5 ng) with or without pFC MEKK (12.5 ng). Different concentrations of nV5-PAGE4 were used to test dosage effect on c-Jun transactivation. Cells were lysed 48 h after transfection using Luciferase lysis buffer (25 mM Tris base, 2 mM EDTA, 10% glycerol, 1% Triton X100. pH adjusted to 7.8 using phosphoric acid) [43]. Dual-Luciferase® Reporter (DLR™) Assay System reagent (Promega, Madison, WI) was added to cell lysate and luciferase activity was recorded on LUMIstar Omega luminescence microplate reader (BMG Labtech GmbH, Ortenberg, Germany). A similar procedure was used for the 3′UTR p27 luciferase promoter [44].

2.8. Quantitative real-time PCR

First strand cDNA from pooled normal adult ($N = 5$) and fetal prostate ($N = 1$) was obtained from BioChain Institute, Inc. (Newark, CA). Quantitative real-time PCR (qPCR) reactions were performed with 0.5 µl of cDNA template in 25 µl of reaction mixture containing 12.5 µl of iQ SYBR Green Supermix (Bio-Rad Laboratories, Inc., Hercules, CA) and 0.25 µmol/l each primer. PCR reactions were subjected to hot start at 95 °C for 3 min followed by 45 cycles of denaturation at 95 °C for 10 s, annealing at 60 °C for 30 s, and extension at 72 °C for 30 s using the CFX96 Real-Time PCR Detection System (Bio-Rad Laboratories, Inc.). PCR primers were 5′- CGTAAAGTAGAAGGTGATTG -3′ (forward) and 5′- ATGCTTAGGATTAGGTGGAG -3′ (reverse) for PAGE4, 5′- TAACAGT GGGTGCCAACTCA -3′ (forward) and 5′- TTTTTCTCTCCGTCGCAACT -3′ (reverse) for c-Jun and 5′- GAATATAATCCCAAGC GGTTTG -3′ (forward) and 5′- ACTTCACATCACAGCTCCCC -3′ (reverse) for TATA binding protein (TBP)[45]. Analysis and fold differences were determined using the comparative threshold cycle method. All experiments were performed in triplicate and data presented represents mean ± SD. Data are presented as mean ± SD and statistical differences between two groups of data were analyzed using the Student's t test. Statistical significance was applied to P values of less than 0.05.

2.9. Immunohistochemistry

The polyclonal PAGE4 antibody WER2 was generated as described previously [46] using the following peptide N-CKTPPNPKHAKTKEAGDGQP-C (Sigma-Gneosys). Immunohistochemical (IHC) staining was conducted using an EnVision™ FLEX System (Dako) according to the manufacturer's protocol with minor modifications. The paraffin section was blocked in 5% skim milk for 1 h and then treated with WER2 rabbit polyclonal antibody that was diluted at 1:1000 for 30 min at room temperature.

3. Results

3.1. Both PAGE4 and c-Jun are overexpressed in the developing prostate

While there is good evidence in the literature supporting upregulation of both PAGE4 and c-Jun in the diseased prostate, not much is known about their co-expression in the developing gland. Therefore, we determined the relative expression of both genes at the mRNA level in the same human fetal prostate samples by qPCR. As shown in
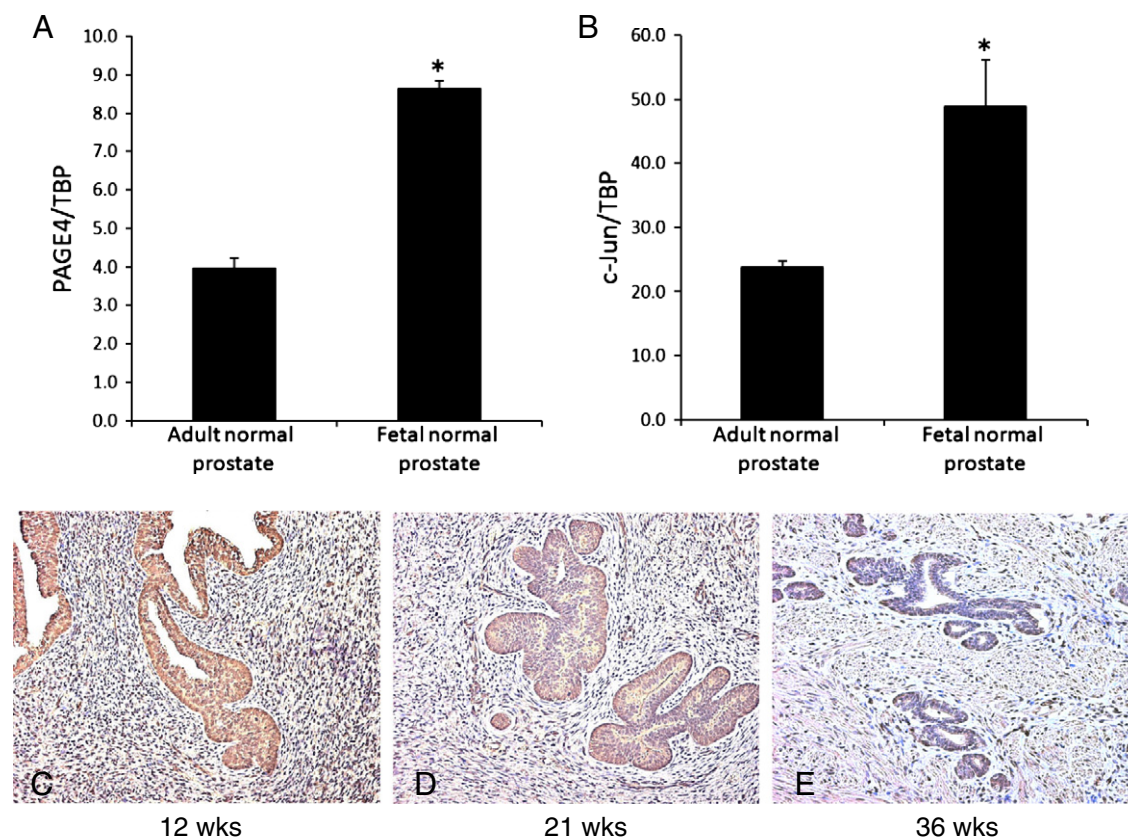
Fig. 1. PAGE4 and c-Jun expression in normal adult and fetal prostate. Messenger RNA levels of PAGE4 (A) and c-Jun (B) were determined in normal adult and fetal prostate by qPCR. Human fetal cDNA was purchased commercially. PAGE4 and c-Jun mRNA expression was normalized to TATA binding protein (TBP). The experiments were repeated three times. Data are represented as mean of triplicate experiments $\pm$ SD. (*$P < 0.01$, Student's t test). (C–E) Fetal prostate was stained for PAGE4 at gestational weeks 12, 21 and 36.

Fig. 1, both PAGE4 (1A) and c-Jun (1B) transcripts are upregulated in the developing prostate when compared to the normal adult prostate. To determine expression at the protein level, paraffin-embedded sections of human fetal prostate tissue obtained from various gestational stages were stained with a PAGE4-specific antibody. As shown in Fig. 1C–E, while the PAGE4 protein is highly expressed in the earlier stages of fetal development, its expression decreases dramatically by the time the pre-pubertal prostate buds are developed (36 weeks). Taken together, the data highlight its potential role in the development of this sex gland.

3.2. Biophysical characterization of the PAGE4 protein

We had previously provided preliminary evidence using a combination of gel electrophoresis, size exclusion chromatography (SEC), circular dichroism (CD) and one dimensional nuclear magnetic resonance (NMR) spectroscopy confirming bioinformatic predictions that PAGE4 is intrinsically disordered [8]. Here, we quantify the SEC results for comparison with dynamic light scattering (DLS) and smFRET measurements to gain additional insight into its ensemble characteristics at the single molecule level.

The SEC results were calibrated against measurements of ovalbumin (MW 43 kD; elution 15.6 ml) and ribonuclease A (MW 13.7 kD; elution 18.3 ml). The hydrodynamic radii (R_h) for these standards were derived from published relationships between R_h and molecular weights for globular proteins [47] and defined as $\log(R_h) = -0.204 + 0.357\log(MW)$ with MW in Daltons and R_h in Angstroms. A linear fit of $\log(R_h)$ versus the elution volume (Ve) for the standards, $\log(R_h) = 2.4748 - 0.65681*Ve$, was used to determine R_h for PAGE4 from its elution volume. The SEC of PAGE4 produced 2 peaks at 14.2 ml and 15.7 ml, suggesting R_h of 3.5 and 2.8 nm. DLS measurements using a Malvern Nanosizer of PAGE4 yielded an $R_h = 3.2 \pm 0.2$ nm (average $\pm$ 1 standard deviation of 3 independent repeated experiments), which is consistent with the R_h measurement using SEC. The large R_h size determined from both SEC and DLS for a protein as small as PAGE4 (only 102 amino acids, 11.15 kDa) is good evidence of the molecule being highly intrinsically disordered. Using published relationships between R_h and molecular weights for disordered proteins in various structural forms [47], R_h is expected to be 1.7 nm if folded globular, 2.8 nm if native unfolded coil-like, and 2.5 nm if native unfolded pre-molten globule. There is good agreement between measured SEC and expected coil-like R_h for disordered PAGE4. The second SEC elution peak is possibly a larger, dimeric PAGE4 form. The measured R_h is close to the 3.3 nm predicted size for the disordered pre-molten globule form of a PAGE4 dimer [47], suggesting that partial compaction may accompany dimerization.

Next, to further examine specific conformational properties of the intrinsic disorder of PAGE4, we developed a smFRET assay. A unique advantage of smFRET is that it can capture information normally lost through ensemble averaging of heterogeneous and dynamic samples. Furthermore, immobilization of single molecules under conditions that retain their biological activity, allows for extended observation of the same molecule for tens of seconds, facilitating the capture of slow conformational transitions or protein binding and unbinding cycles. Finally, the use of an open geometry for immobilization permits direct observation of the response to changing solution conditions or adding ligands.

We generated 2 different cysteine (Cys) mutants of PAGE4 that were labeled with donor and acceptor fluorophores for FRET studies. Cysteine residues were introduced near the N terminus or C terminus of the 102 amino acid long PAGE4 molecule at positions 18 or 102 by replacing an Ala (A18C) and Pro (P102C) residue, respectively. These mutants alternately combined with the single native Cys residue at position 63 to

generate two double cysteine constructs (Fig. 2A) were simultaneously labeled with Alexa Fluor 555 (AF555, FRET donor) and Alexa Fluor 647 (AF647, FRET acceptor) resulting in random attachment of donor and acceptor on the cysteines. Protein molecules emitting fluorescence indicating that exactly 1 donor and 1 acceptor were isolated for further analysis. The mutant PAGE4 polypeptides were labeled efficiently with the donor/acceptor dyes and the labeled samples ran as a single band of the expected molecular weight in SDS-PAGE analysis (Supplementary Fig. 1).

We immobilized the PAGE4 FRET mutants on a surface to allow extended smFRET measurements. Widely spaced streptavidin molecules were deposited on quartz slides and the intervening spaces were passivated by lipid bilayers [48]. Next, biotinylated antibodies to 6His tags (Thermo Scientific Cat #: MA1-80087) were bound on the surface adhered streptavidin. Finally, PAGE4 was immobilized on the antibodies via its N-terminal 6His tag. Single molecule FRET signals were measured from these surface tethered PAGE4 samples (see Methods). Time trajectories of donor and acceptor emission intensities (Id and Ia respectively) from individual molecules were steady until single step photobleaching events (Fig. 2) that confirmed single molecule detection. FRET efficiency calculated from the intensities as $E = Ia/(Ia + Id)$ and FRET ratio histograms made from E for many molecules were consistent with rapid motion of the donor and acceptor attachment locations around Root Mean Square (RMS) distances as expected for IDPs. In particular, the widths of the histograms were shot noise limited indicating the motion was much faster than that of the 100 millisecond sampling time. To test for possible undesirable interactions with the surface we compared FRET measurements of PAGE4 directly tethered to the surface coated with 6His antibodies to FRET measurements of PAGE4 encapsulated inside 100 nm diameter liposomes, which were tethered to the surface [38,49]. Gaussian fits (center ± sigma) to the histograms were nearly unchanged for direct immobilization and liposome encapsulated for both A18C/63C (direct $E = 0.56 \pm 0.17$; encapsulated $E = 0.55 \pm 0.17$) and P102/63C (direct $E = 0.65 \pm 0.18$; encapsulated $E = 0.65 \pm 0.17$) mutants. Of particular note, in contrast to some other IDPs [38], no slow conformational switching was observed in PAGE4 (Fig. 2C–F).

We used these FRET measurements to estimate a scale characterizing the size of disordered PAGE4. For conversion of measured FRET efficiency into distance, we determined that the γ factor was 0.96 for the A18C/63C mutant and 1.13 for the P102C/63C. Therefore, we used $\gamma = 1$ as a global correction [41] and a Förster radius of 5.24, which is a value used in the literature for this dye pair [50]. As described elsewhere, we used a Gaussian probability distribution for the RMS distance between the cysteines used for dye attachment to recover the R_{RMS} from the experimentally determined dye separations from FRET [38]. This analysis yielded $R_{RMS} = 5.52$ nm for A18C/63C FRET and $R_{RMS} = 4.95$ nm for P102C/63C FRET. Using 0.36 nm per amino acid, we determined the contour length of the protein chain between the dye-labeled cysteines to be 16.2 nm (A18C/63C) and 14.04 nm (P102C/63C). The measured R_{RMS} and contour length between the donor and acceptor attachment sites can be used with the random polymer model ($R_{RMS}^2 = 2l_pL$) [51,52] to determine the persistence length (l_p) of the intervening protein as 0.94 nm (A18C/63C) and 0.87 nm (P102C/63C). The expected R_{RMS} for the whole protein is then estimated to be 8.3 nm or 8.0 nm by using the A18C/63C or P102C/63C l_p values with the 36.7 nm contour length of the full-length protein of 102 amino acids. Radius of gyration (R_G) estimates derived from R_{RMS} ($R_G = R_{RMS}/\sqrt{6}$) are 3.39 and 3.27 nm for A18C/63C and P102C/63C, respectively. The radius of gyration estimates allows 4 comparisons of the ratios of gyration radius to hydrodynamic radius (R_G/R_h) using R_h from gel filtration (2.8 nm) and DLS (3.2 nm). These are 1.21, 1.17, 1.06 and 1.02 (average 1.12, SD 0.09). The average of these values compares well with a study of an array of chemically denatured proteins where the average $R_G/R_h = 1.06$ was found [53]. These comparisons of smFRET derived characterizations with hydrodynamic characterizations further confirm that PAGE4 is a highly disordered protein.

3.3. Identifying PAGE4 interacting partners

Although the smFRET results indicated lack of stochastic conformational fluctuations, it is plausible that the PAGE4 molecule switches conformations upon interacting with a biological target (coupled folding and binding). Therefore, we next focused on identifying protein partners that may interact with PAGE4 so that they could be used as ligands in the smFRET assay. To this end we employed the yeast two hybrid system as described in the Materials & Methods. Briefly, the PAGE4
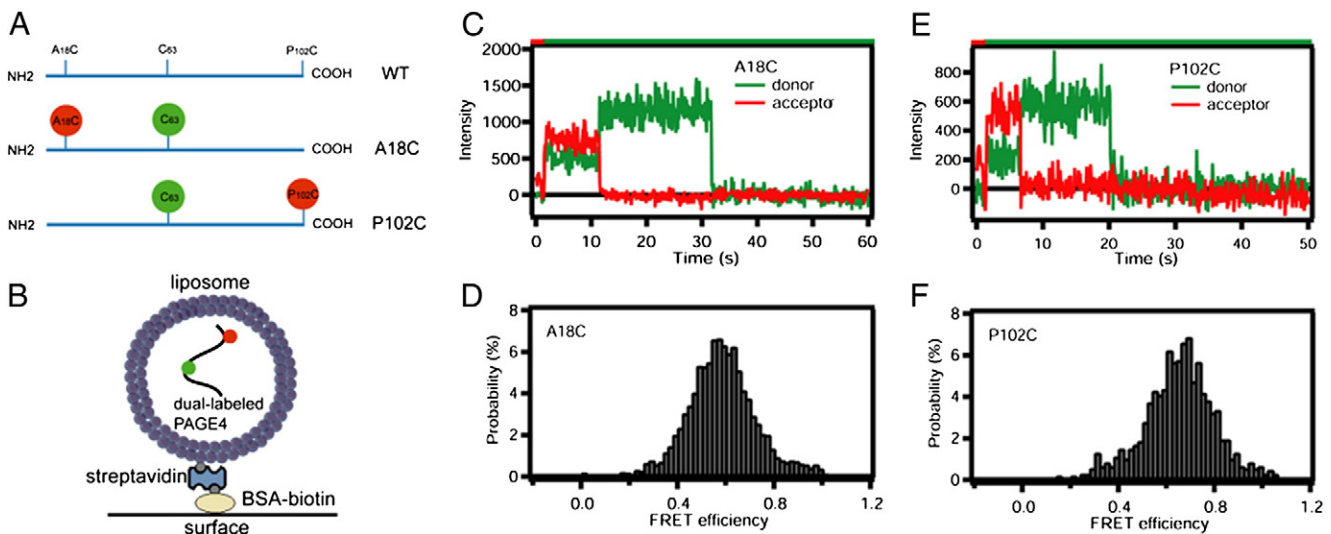

Fig. 2. Single molecule FRET indicates that PAGE4 is an intrinsically disordered protein. (A) Schematic of the PAGE4 constructs with the native cysteine (green) and the introduced cysteine (red). Single PAGE4 protein molecules were encapsulated inside 100 nm diameter liposomes tethered to a quartz surface. (B) Shows a cartoon of this immobilization scheme (not to scale). Fluorescence emission timecourses in the donor and acceptor spectral bands were collected and those indicating exactly 1 donor and 1 acceptor were further analyzed. Example intensity timecourses showing anti-correlated donor/acceptor behavior upon photobleaching, which is characteristic of single molecules, are shown for the A18C/63C (C) and P102C/63C (E) FRET mutants. The color bar at the top indicates the illumination color. Red illumination at the start driving only acceptor fluorescence allows identification of molecules containing an active acceptor. The disappearance of red emission (with anticorrelated recovery of green) is photobleaching of the acceptor, and disappearance of green emission is photobleaching of the donor. Histograms assembled from all FRET active data points of over 300 molecules are shown for A18C/63C (D) and P102C/63C (F) PAGE4 mutants. These FRET signals agree with expectations based upon modeling PAGE4 as a highly flexible IDP.

molecule fused in frame to the GAL4 DNA binding domain (GAL4-DBD) served as the bait and a PCa cDNA library fused in frame to the GAL4 activation domain (GAL4-AD) as the prey. This screen resulted in several colonies on double dropout (Leu⁻, Trp⁻) plates but only one colony was positive when plated on quadruple dropout (Leu⁻, Trp⁻, Ade⁻, His⁻) plates containing X-α-gal (Supplemental Fig. 2) suggesting that this clone represents a putative PAGE4 interacting partner. Sequencing of the plasmid insert from the quadruple positive clone showed that this plasmid contained the cDNA encoding the human ZNF394 sequence.

ZNF394 is a 64 kDa zinc finger protein that is specifically expressed in the heart, skeletal muscle, and brain in adult human tissues [54]. Overexpression of ZNF394 in COS-7 cells inhibits the transcriptional activities of c-Jun and AP-1 reporters, suggesting that ZNF394 is a transcriptional repressor in the MAP kinase signaling pathway and may play an important role in cardiac development and/or cardiac function. To confirm the yeast two hybrid data, we set up the c-Jun/AP-1 reporter system in the PC3 PCa cell line. As shown in Supplemental Fig. 3, GAL4-c-Jun in the presence of MEKK, showed a robust activation of the reporter gene. But in contrast to the results of Huang et al. in COS-7 cells [54], ZNF394 did not repress c-Jun activity in PC3 cells. Surprisingly, however, the addition of PAGE4 further enhanced the activity of c-Jun suggesting that PAGE4 may directly interact with c-Jun instead.

3.4. PAGE4 potentiates transactivation of the proto-oncogene c-Jun

To test the effect of PAGE4 on c-Jun transactivation, we used a reporter gene assay. We titrated various concentrations of nV5-PAGE4 with DNA-binding domain (DBD) of the yeast protein GAL4 (aa1-147) fused in-frame to the transactivation domain of c-Jun (aa 1-223) in PC3 cells. As shown in Fig. 3, the results clearly indicate that PAGE4 potentiates c-Jun transactivation in a dosage-dependent manner. To test the overall effect on the activation of JNK pathway, we co-expressed the kinase domain of human MEKK protein (aa 380-672) in the presence of different concentrations of PAGE4. MEKK is a Serine/Threonine-specific MAPKKK that activates JNK pathway [55]. MEKK along with JNKK activate JNK which phosphorylates and transcriptionally activates c-Jun [56]. Interestingly, in the presence of MEKK and PAGE4, luciferase

activity was increased by ~600 fold as compared to empty vector/control as shown in Fig. 3. Therefore, we conclude that PAGE4 potentiates c-Jun transactivation in a MEKK-JNK-dependent manner. However, a PAGE4 GAL4 fusion construct failed to transactivate the luciferase reporter gene (not shown). These data strongly suggest but do not necessarily prove that PAGE4 directly interacts with c-Jun but by itself is not a bona fide transcription factor.

3.5. c-Jun induces conformational changes in PAGE4 upon binding

We used smFRET to further characterize the c-Jun interaction with PAGE4. To this end, the FRET reporting donor/acceptor labeled PAGE4 double cysteine mutants were immobilized on a surface through binding of the N-terminal 6His tag to a biotinylated 6His antibody attached to streptavidin on the surface (Fig. 4A).

The FRET values from PAGE4 changed substantially upon addition of 40 μg/ml (1.6 μM) of a commercially obtained, bacterially expressed fragment of truncated c-Jun (aa 1-241; ProSpec, catalog number PKA-001). FRET from the N-terminal label pair A18C/63C shifted higher while FRET from the C-terminal P102C/63C mutant shifted lower (Fig. 4) indicating interaction between c-Jun and PAGE4. We fit the FRET histograms with sums of 2 Gaussians where one Gaussian matched the free PAGE4 experiment to account for partial saturation of the c-Jun/PAGE4 interaction. The new Gaussians that emerged had widths consistent with expectations due to experimental conditions (Methods and Supplementary Table 1) and had centers that were shifted from the free PAGE4 value by more than the typical run to run variation of control experiments (A18C/63C: 0.56 without c-Jun, 0.61 with c-Jun; P102C/63C: 0.65 without c-Jun, 0.39 with c-Jun), suggesting a distinct conformational state. To discern the contribution of the c-terminal domain of the c-Jun molecule that comprises the DNA-binding and dimerization domains (the basic leucine zipper region) in the interaction with PAGE4, bacterially expressed and purified full-length c-Jun protein was added at the same concentration. The new FRET peak for both truncated and full-length c-Jun consistently shifts in FRET values from free PAGE4 FRET peaks (A18C/63C: 0.56 without c-Jun, 0.62 truncated c-Jun, 0.80 full length c-Jun; P102C/63C: 0.65 without c-Jun, 0.39 truncated c-Jun, 0.37 full length c-Jun) (Fig. 4C &
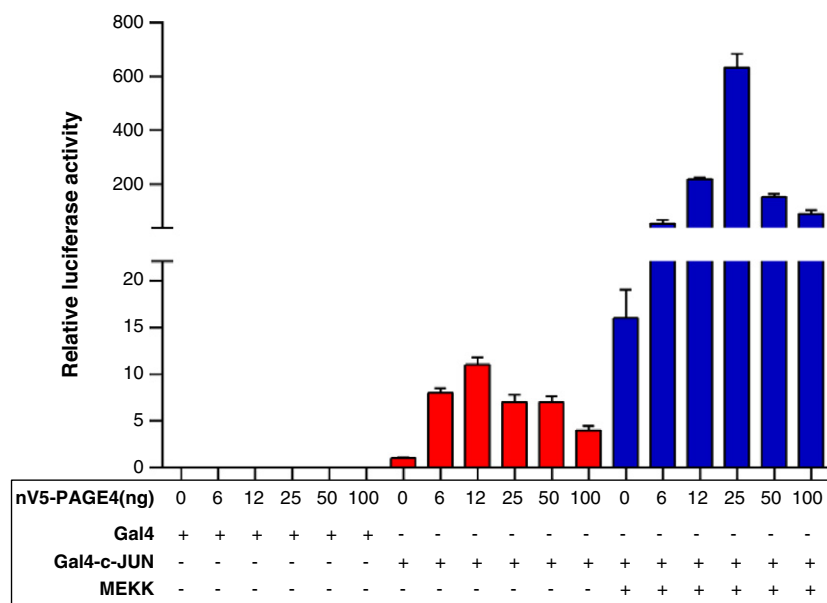

Fig. 3. PAGE4 potentiates the c-Jun activity. GAL4 (aa 1-147) or GAL4-cJUN (aa 1-223) was cotransfected with or without MEKK and various amounts of V5-tagged PAGE4 (nV5-PAGE4) into PC3 cells. The V5 epitope tag is a small epitope (GKPIPNPLLGLDST) that is derived from the P and V proteins of the paramyxovirus of simian virus 5 and was fused in-frame at the N terminus. Luciferase activities from a GAL4 binding site-driven reporter construct were measured and plotted with reference value normalized to 1.
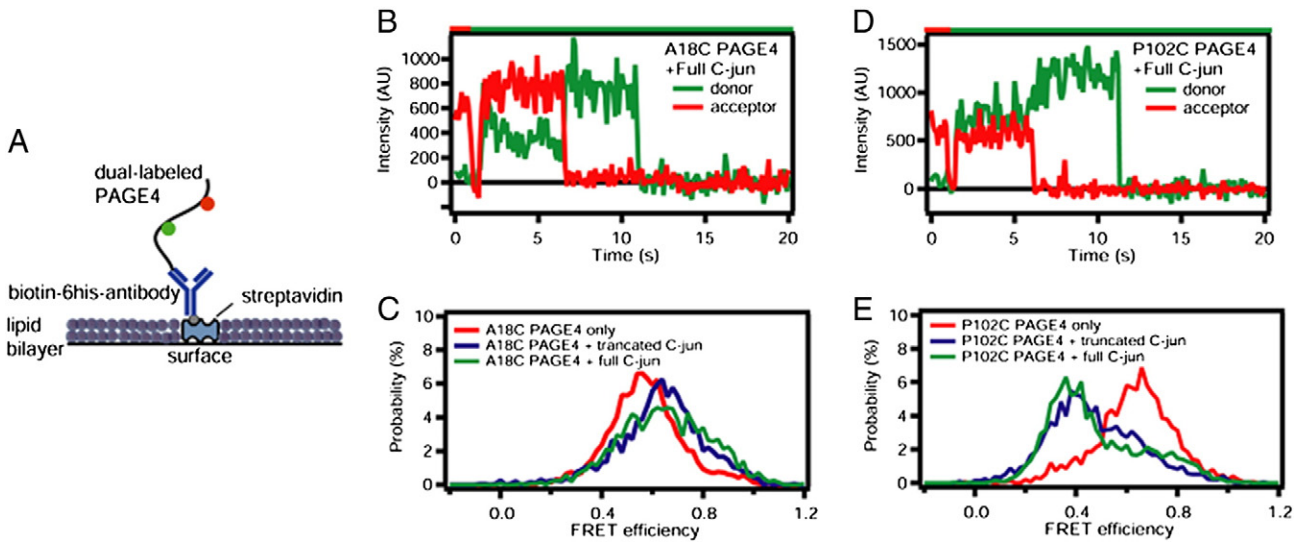
Fig. 4. Single molecule FRET indicates interaction with c-Jun alters the conformation of PAGE4. Alexa555/Alexa647 labeled PAGE4 containing a 6His tag was directly immobilized on a quartz surface with widely spaced streptavidin molecules adhered, which were used to link to biotinylated-6-His-antibodies. The space between streptavidins was passivated with a lipid bilayer. (A) Displays a cartoon of this immobilization scheme (not to scale). Single molecule fluorescence time traces for donor and acceptor emission were analyzed from molecules confirmed to contain exactly 1 donor and 1 acceptor for the A18C/63C (panel B) and P102C/63C (panel D) FRET mutants in the absence of c-Jun. The color bar at the top indicates the illumination color. Histograms assembled from all FRET active data points of over 300 molecules are shown as the red curves for A18C/63C (panel C) and P102C/63C (panel E) PAGE4 mutants. Note FRET measurements of liposome encapsulated PAGE4 (Fig. 2) agree with the FRET measured from this directly surface immobilized PAGE4. The blue curves are FRET histograms from PAGE4 in the presence of 0.4 mg/ml truncated c-Jun for the A18C/63C (panel C) and P102C/63C (panel E) PAGE4 mutants. C-Jun causes FRET to increase for A18C/63C mutant and to decrease for P102C/63C mutant. The green curves in C and E are for full-length c-Jun.

E). Both truncated and full-length c-Jun led to consistent increases in FRET for PAGE4 A18C/63C and consistent decreases in FRET for PAGE4 P102C/63C, suggesting that interaction of PAGE4 with c-Jun is mediated via the proximal portion of the molecule that harbors the transactivation domain [57].

To rule out potential experimental artifacts due to crowding or non-specific binding, we measured smFRET after including 100 μg/ml of bovine serum albumin (BSA) with PAGE4. However, this caused no change in FRET in either mutant (Fig. 5, with BSA) ruling out simple non-specific crowding as causing FRET changes. To interrogate for possible interactions directly with the fluorophores, we measured
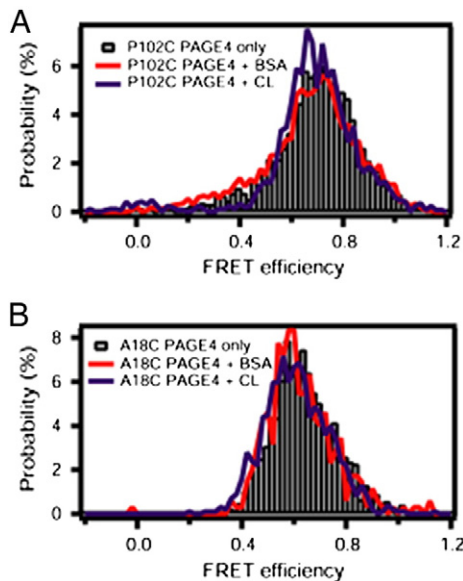

Fig. 5. Crowding and lipid interactions do not alter PAGE4 conformation. Histograms of single molecule FRET signals from surface immobilized PAGE4 (gray bars) are unchanged from single molecule FRET histograms of surface immobilized PAGE4 in the presence of 0.1 mg/ml bovine serum albumin (red curve) or 20% cardiolipin containing PC liposomes (blue curve) for both the P102C/63C (A) and A18C/63C (B) PAGE4 mutants.

effects of c-Jun on fluorescence anisotropy and quantum yield (QY) of Alexa 555 attached to PAGE4. Fluorescence anisotropy measurements confirmed that c-Jun did not dramatically alter dye mobility. The fluorescence anisotropy of PAGE4 labeled with only Alexa 555 did not change for either wild type protein containing only the native centrally located cysteine (0.248 without c-Jun, 0.242 with c-Jun) or the double cysteine mutants (with very low labeling efficiency so that nearly all molecules only contain one Alexa 555 randomly distributed between the cysteine) A18C/63C (0.257 without c-Jun, 0.250 with c-Jun) and P102C/63C (0.244 without c-Jun, 0.250 with c-Jun). In contrast, interactions with c-Jun caused changes in the quantum yield (QY) of Alexa 555 attached to all cysteines used in our studies. The ratio of QY after adding full-length c-Jun to QY before adding c-Jun was 1.24 (WT), 1.27 (A18C/63C) and 1.38 (P102C/63C). The FRET γ-factor, which is sensitive to the ratio of acceptor QY to donor QY, changed from +3% to −12% upon c-Jun exposure for the various experimental permutations (Methods). In combination, the change in donor QY and FRET γ-factor suggests that the acceptor QY also changes on the order of 10% upon c-Jun binding.

Changes in donor QY in the absence of conformational change will cause FRET efficiency to change because the Förster radius parameter depends on the 1/6 power of the donor QY. Consideration of how donor QY affects FRET demonstrates this phenomenon is not causing the FRET change we observe in our experiment. Neglecting the coincident change in γ-factor (that shifts FRET efficiency in the opposite direction from the effect we are considering due to changing donor QY altering the Förster radius parameter), it may be shown that upon a change in donor QY from $\Phi_{donor,\ old}$ to $\Phi_{donor,\ new}$ the change in FRET efficiency from E_{old} to E_{new} is

$$E_{new} = 1 / \left\{ 1 + \left(\Phi_{donor,old} / \Phi_{donor,new} \right) * \left((1/E_{old}) - 1 \right) \right\}.$$

Using $(\Phi_{donor,\ new} / \Phi_{donor,\ old}) = 1.2$ (which is the scale of QY change we measured), this analysis predicts the expected changes in FRET efficiency for A18C/63C is +0.0443 and for P102C/63C is +0.0403. We observed change in FRET of −0.15 (A18C/63C) and +0.27 (P102C/63C). The much larger changes in FRET than expected from

the change in donor QY considered in combination with the γ-factor and anisotropy results provide strong support to the interpretation that c-Jun substantially alters the global configuration of PAGE4. More intuitively, it can be simply stated that increases in donor QY as we measured for both labeled constructs will increase measured FRET efficiency when fluorophore separation does not change. In our experiments, FRET increases for the P102/63C construct but decreases for A18C/63C construct, which is only possible if c-Jun causes conformational changes in PAGE4.

We also explored an additional line of evidence to demonstrate specificity. Upon exposing PCa cell lines to stressful conditions such as nutrient deprivation for example, there is a significant increase in mitochondrial-associated PAGE4 and a concomitant decrease in cytoplasmic levels of PAGE4 (Zeng et al., unpublished). In a recent publication, Zigoneanu et al. [58] observed that the IDP α-synuclein interacts strongly with large unilamellar vesicles whose composition is similar to that of the inner mitochondrial membrane, which contains cardiolipin. Therefore, to test for possible interactions between cardiolipin and PAGE4, we encapsulated the donor/acceptor labeled PAGE4 constructs inside liposomes consisting of 80%PC/20% cardiolipin. As shown in Fig. 5A and B, we measured FRET signals from both the A18C/63C and P102C/63C donor/acceptor labeled FRET mutants of PAGE4 inside 20% cardiolipin liposomes that were unchanged from surface tethered or 100% PC liposome encapsulated experiments. Collectively, these data suggest that although PAGE4 relocalizes to the mitochondrion under stress, it does not interact with cardiolipin in the mitochondrial inner membrane, or if it does, cardiolipin does not induce substantial conformational changes in PAGE4. These observations underscore the significance of PAGE4 interactions with c-Jun.

3.6. PAGE4 modulates expression of the c-Jun targets mir221/222 that target p27 in prostate cancer

MicroRNAs (miRNAs) are potent negative regulators of gene expression and are frequently implicated in many types of cancer including PCa. While some miRNAs are upregulated and thought to function as oncogenic, others that are downregulated are believed to act as tumor suppressors. Mir-221 and miR-222 are two closely related miRNAs that are encoded in cluster from a genomic region on chromosome X and are strongly upregulated in many cancers where they were shown to play an oncogenic role via the downregulation of several tumor suppressors such as p27, p57, PTEN and many others [59,60]. The expression of these miRNAs in PCa cells is thought to be driven by the cooperative interaction of NFkB and c-Jun on two separate distal regions upstream of miR-221/222 promoter [61]. Therefore, we reasoned that if PAGE4 potentiates c-Jun transactivation, one would observe an increase in the down regulation of the mir221/222 targets. To test this possibility, we conducted a luciferase reporter assay in PC3 cells with the wild type or mutant p27 3′UTR in which the mir221/222 binding sites were scrambled and fused to the luciferase reporter. As shown in Fig. 6, overexpressing PAGE4 resulted in ~50% decrease in the reporter activity; however, ~10% decrease was observed with the mutant reporter suggesting that in PCa cells, PAGE4 by potentiating c-Jun transactivation contributes to tumorigenesis by downregulating tumor suppressors such as p27.

4. Discussion

Considered together, our results demonstrating that PAGE4 interacts with c-Jun to potentiate its transactivation, and that this interaction induces conformational changes in PAGE4, have significant implications. From a fundamental perspective, recent research on IDPs and how they might contribute to pathological states when overexpressed suggests that noise in PINs contributed by the conformational dynamics of IDPs plays a critical role in information transfer in cancer[32]. Since many IDPs transition from disorder to order upon binding to their
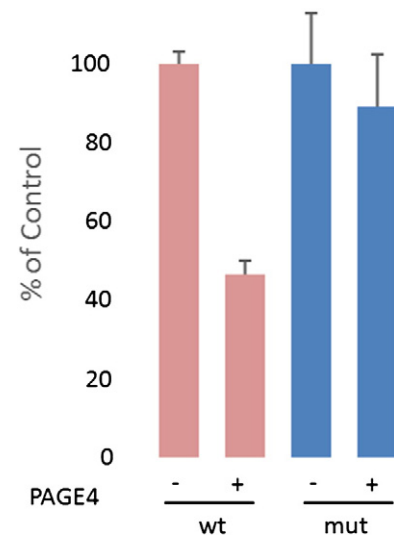

Fig. 6. PAGE4 expression causes down-regulation of p27 in PC3 cells. A luciferase reporter assay was conducted with either wild type (wt) or mutant (mut) p27 3′UTR fused to luciferase. The mut vector had the mir221/222 binding sites scrambled. The assay was done in quadruplicate and the empty vector was normalized to 100%.

target, stochasticity of IDP interactions allows the system to search through numerous iterations of network interactions and select those that increase fitness. Rewiring of noise-driven PINs can activate latent pathways that drive cellular transformation and adaptation [32]. Thus, given the potential for conformational flexibility, PAGE4 could rewire PINs by interacting with multiple partners and drive cellular transformation. It is noteworthy that to date, no activating mutations have been reported for any of the bona fide CTAs, a majority of which are IDPs [7] and are overexpressed in several types of cancer.

From a medical perspective, several lines of evidence have illustrated the importance of c-Jun overexpression in both benign prostatic hyperplasia (BPH) and PCa. First, c-Jun is a coactivator of the androgen receptor (AR) [62–64], a key player in both BPH [65]as well as PCa [62,66]. c-Jun stimulates AR transactivation by mediating receptor dimerization and subsequent DNA binding [63]. Interestingly, c-Jun also enhances AR transactivation in androgen-independent PCa cells, which closely mimic hormone-refractory PCa cells in gene expression and growth behavior [66]. Furthermore, repression of endogenous c-Jun expression results in markedly reduced growth of these cells, strongly suggesting an important biological role for c-Jun in hormone-refractory PCa. Second, c-Jun, by acting on the distal enhancer region, cooperates with other factors to induce expression of the oncogenic microRNAs miR-221/222 [67]. Mir-221 and miR-222, two closely related microRNAs encoded in a cluster from a genomic region on chromosome X, are strongly upregulated in several forms of human tumors including PCa [67]. Third, like PAGE4, c-Jun is also expressed in BPH, underscoring the functional significance of the PAGE4/c-Jun interaction. The c-Jun protein in prostate fibroblasts regulates production and paracrine signals of insulin-like growth factor-1 (IGF-1) which stimulate BPH-1 cellular proliferation. In addition, stromally produced IGF-1 upregulates epithelial mitogen-activated protein kinase, Akt, and cyclin D1 protein levels while downregulating the cyclin-dependent kinase inhibitor p27. Together these data suggest that stromally expressed c-Jun may promote prostatic epithelial proliferation through IGF-1 as a paracrine signal that, in turn, can promote prostate epithelial proliferation [65]. Finally, the role of c-Fos and c-Jun in PCa progression and recurrence has been elegantly demonstrated both in transgenic mouse models as well as in human PCa. Thus, forced expression of c-Fos and c-Jun in PCa cells promotes tumorigenicity and results in activation of an extracellular signal-regulated kinase signaling. Additionally, up-regulation of both c-Fos and c-Jun proteins occurs in advanced disease is correlated with extracellular signal-regulated kinase pathway activation [68]. Taken

together, our findings that PAGE4 interacts with c-Jun, which is an important player in human PCa, and potentiates its transactivation reveal a hitherto unappreciated role for this CTA in PCa.

It is important to note that c-Jun typically heterodimerizes with c-Fos, and together they constitute a member of the AP-1 family of transcription factors [69,70]. Thus, it will be important to determine whether PAGE4 interacts with c-Jun alone or with the Jun/Fos heterodimer and how this interaction could affect its ability to potentiate AP-1 transactivation. Nonetheless, the present study suggests that disrupting PAGE4/c-Jun interactions using small molecules may serve as a promising therapeutic opportunity for BPH as well as PCa which are among the most common ailments in the aging male population worldwide.

Supplementary data to this article can be found online at http://dx.doi.org/10.1016/j.bbadis.2013.11.014.

References

[1] P. Kulkarni, T. Shiraishi, K. Rajagopalan, R. Kim, S.M. Mooney, R.H. Getzenberg, Cancer/testis antigens and urological malignancies, Nat. Rev. Urol. 9 (2012) 386–396.
[2] A.J. Simpson, O.L. Caballero, A. Jungbluth, Y.T. Chen, L.J. Old, Cancer/testis antigens, gametogenesis and cancer, Nat. Rev. Cancer 5 (2005) 615–625.
[3] M.J. Scanlan, A.O. Gure, A.A. Jungbluth, L.J. Old, Y.T. Chen, Cancer/testis antigens: an expanding family of targets for cancer immunotherapy, Immunol. Rev. 188 (2002) 22–32.
[4] T. Suyama, T. Shiraishi, Y. Zeng, W. Yu, N. Parekh, R.L. Vessella, J. Luo, R.H. Getzenberg, P. Kulkarni, Expression of cancer/testis antigens in prostate cancer is associated with disease progression, Prostate 70 (2010) 1778–1787.
[5] N. Sampson, C. Ruiz, C. Zenzmaier, L. Bubendorf, P. Berger, PAGE4 positivity is associated with attenuated AR signaling and predicts patient survival in hormone-naive prostate cancer, Am. J. Pathol. 181 (2012) 1443–1454.
[6] W.G. Nelson, A.M. De Marzo, W.B. Isaacs, Prostate cancer, N. Engl. J. Med. 349 (2003) 366–381.
[7] K. Rajagopalan, S.M. Mooney, N. Parekh, R.H. Getzenberg, P. Kulkarni, A majority of the cancer/testis antigens are intrinsically disordered proteins, J. Cell. Biochem. 112 (2011) 3256–3267.
[8] Y. Zeng, Y. He, F. Yang, S.M. Mooney, R.H. Getzenberg, J. Orban, P. Kulkarni, The cancer/testis antigen prostate-associated gene 4 (PAGE4) is a highly intrinsically disordered protein, J. Biol. Chem. 286 (2011) 13985–13994.
[9] V.N. Uversky, Unusual biophysics of intrinsically disordered proteins, Biochim. Biophys. Acta 1834 (2013) 932–951.
[10] P. Tompa, Intrinsically disordered proteins: a 10-year recap, Trends Biochem. Sci. 37 (2012) 509–516.
[11] V.N. Uversky, C.J. Oldfield, A.K. Dunker, Intrinsically disordered proteins in human diseases: introducing the D2 concept, Annu. Rev. Biophys. 37 (2008) 215–246.
[12] A. Patil, K. Kinoshita, H. Nakamura, Hub promiscuity in protein–protein interaction networks, Int. J. Mol. Sci. 11 (2010) 1930–1943.
[13] C. Haynes, C.J. Oldfield, F. Ji, N. Klitgord, M.E. Cusick, P. Radivojac, V.N. Uversky, M. Vidal, L.M. Iakoucheva, Intrinsic disorder is a common feature of hub proteins from four eukaryotic interactomes, PLoS Comput. Biol. 2 (2006) e100.
[14] P. Tompa, P. Csermely, The role of structural disorder in the function of RNA and protein chaperones, FASEB J. 18 (2004) 1169–1175.
[15] Y.J. Edwards, A.E. Lobley, M.M. Pentony, D.T. Jones, Insights into the regulation of intrinsically disordered proteins in the human proteome by analyzing sequence and gene expression data, Genome Biol. 10 (2009) R50.
[16] M.M. Babu, R. van der Lee, N.S. de Groot, J. Gsponer, Intrinsically disordered proteins: regulation and disease, Curr. Opin. Struct. Biol. 21 (2011) 432–440.
[17] M.K. Yoon, V. Venkatachalam, A. Huang, B.S. Choi, C.M. Stultz, J.J. Chou, Residual structure within the disordered C-terminal segment of p21(Waf1/Cip1/Sdi1) and its implications for molecular recognition, Protein Sci. 18 (2009) 337–347.

[18] A. Nath, M. Sammalkorpi, D.C. DeWitt, A.J. Trexler, S. Elbaum-Garfinkle, C.S. O'Hern, E. Rhoades, The conformational ensembles of alpha-synuclein and tau: combining single-molecule FRET and simulations, Biophys. J. 103 (2012) 1940–1949.
[19] D.S. Libich, G. Harauz, Backbone dynamics of the 18.5 kDa isoform of myelin basic protein reveals transient alpha-helices and a calmodulin-binding site, Biophys. J. 94 (2008) 4847–4866.
[20] C.W. Lee, J.C. Ferreon, A.C. Ferreon, M. Arai, P.E. Wright, Graded enhancement of p53 binding to CREB-binding protein (CBP) by multisite phosphorylation, Proc. Natl. Acad. Sci. U. S. A. 107 (2010) 19290–19295.
[21] C.W. Lee, M. Arai, M.A. Martinez-Yamout, H.J. Dyson, P.E. Wright, Mapping the interactions of the p53 transactivation domain with the KIX domain of CBP, Biochemistry 48 (2009) 2115–2124.
[22] F. Huang, S. Rajagopalan, G. Settanni, R.J. Marsh, D.A. Armoogum, N. Nicolaou, A.J. Bain, E. Lerner, E. Haas, L. Ying, A.R. Fersht, Multiple conformations of full-length p53 detected with single-molecule fluorescence resonance energy transfer, Proc. Natl. Acad. Sci. U. S. A. 106 (2009) 20758–20763.
[23] A. Grupi, E. Haas, Segmental conformational disorder and dynamics in the intrinsically disordered protein alpha-synuclein and its chain length dependence, J. Mol. Biol. 405 (2011) 1267–1283.
[24] A.C. Ferreon, Y. Gambin, E.A. Lemke, A.A. Deniz, Interplay of alpha-synuclein binding and conformational switching probed by single-molecule fluorescence, Proc. Natl. Acad. Sci. U. S. A. 106 (2009) 5645–5650.
[25] C. Andresen, S. Helander, A. Lemak, C. Fares, V. Csizmok, J. Carlsson, L.Z. Penn, J.D. Forman-Kay, C.H. Arrowsmith, P. Lundstrom, M. Sunnerhagen, Transient structure and dynamics in the disordered c-Myc transactivation domain affect Bin1 binding, Nucleic Acids Res. 40 (2012) 6353–6366.
[26] T. Vavouri, J.I. Semple, R. Garcia-Verdugo, B. Lehner, Intrinsic protein disorder and interaction promiscuity are widely associated with dosage sensitivity, Cell 138 (2009) 198–208.
[27] L.M. Iakoucheva, C.J. Brown, J.D. Lawson, Z. Obradovic, A.K. Dunker, Intrinsic disorder in cell-signaling and cancer-associated proteins, J. Mol. Biol. 323 (2002) 573–584.
[28] E.M. Marcotte, M. Tsechansky, Disorder, promiscuity, and toxic partnerships, Cell 138 (2009) 16–18.
[29] B. Munsky, G. Neuert, A. van Oudenaarden, Using gene expression noise to understand gene regulation, Science 336 (2012) 183–187.
[30] Y. Taniguchi, P.J. Choi, G.W. Li, H. Chen, M. Babu, J. Hearn, A. Emili, X.S. Xie, Quantifying *E. coli* proteome and transcriptome with single-molecule sensitivity in single cells, Science 329 (2010) 533–538.
[31] J.E. Ladbury, S.T. Arold, Noise in cellular signaling pathways: causes and effects, Trends Biochem. Sci. 37 (2012) 173–178.
[32] G. Mahmoudabadi, K. Rajagopalan, R.H. Getzenberg, S. Hannenhalli, G. Rangarajan, P. Kulkarni, Intrinsically disordered proteins and conformational noise: implications in cancer, Cell Cycle 12 (2013) 26–31.
[33] S.M. Mooney, A. Goel, A.B. D'Assoro, J.L. Salisbury, R. Janknecht, Pleiotropic effects of p300-mediated acetylation on p68 and p72 RNA helicase, J. Biol. Chem. 285 (2010) 30443–30452.
[34] H.A. O'Neill, O. Gakh, S. Park, J. Cui, S.M. Mooney, M. Sampson, G.C. Ferreira, G. Isaya, Assembly of human frataxin is a mechanism for detoxifying redox-active iron, Biochemistry 44 (2005) 537–545.
[35] S. Park, O. Gakh, S.M. Mooney, G. Isaya, The ferroxidase activity of yeast frataxin, J. Biol. Chem. 277 (2002) 38589–38595.
[36] J.J. Kim, B. Yin, C.S. Christudass, N. Terada, K. Rajagopalan, B. Fabry, D.Y. Lee, T. Shiraishi, R.H. Getzenberg, R.W. Veltri, S.S. An, S.M. Mooney, Acquisition of paclitaxel resistance is associated with a more aggressive and invasive phenotype in prostate cancer, J. Cell. Biochem. 114 (2013) 1286–1293.
[37] J.R. Lakowicz, Principles of Fluorescence Spectroscopy, 3rd ed. Springer, New York, 2006.
[38] U.B. Choi, J.J. McCann, K.R. Weninger, M.E. Bowen, Beyond the random coil: stochastic conformational switching in intrinsically disordered proteins, Structure 19 (2011) 566–576.
[39] U.B. Choi, K.R. Weninger, M.E. Bowen, Immobilization of proteins for single-molecule fluorescence resonance energy transfer measurements of conformation and dynamics, Methods Mol. Biol. 896 (2012) 3–20.
[40] Y. Li, G.J. Augustine, K. Weninger, Kinetics of complexin binding to the SNARE complex: correcting single molecule FRET measurements for hidden events, Biophys. J. 93 (2007) 2178–2187.
[41] J.J. McCann, U.B. Choi, L. Zheng, K. Weninger, M.E. Bowen, Optimizing methods to recover absolute FRET efficiency from immobilized single molecules, Biophys. J. 99 (2010) 961–970.
[42] I.V. Gopich, A. Szabo, Photon counting histograms for diffusing fluorophores, J. Phys. Chem. B 109 (2005) 17683–17688.
[43] S.M. Mooney, J.P. Grande, J.L. Salisbury, R. Janknecht, Sumoylation of p68 and p72 RNA helicases affects protein stability and transactivation potential, Biochemistry 49 (2010) 1–10.
[44] S. Galardi, N. Mercatelli, E. Giorda, S. Massalini, G.V. Frajese, S.A. Ciafre, M.G. Farace, miR-221 and miR-222 expression affects the proliferation potential of human prostate carcinoma cell lines by targeting p27Kip1, J. Biol. Chem. (2007) 23716–23724.
[45] N. Terada, T. Shiraishi, Y. Zeng, S.M. Mooney, D.B. Yeater, L.A. Mangold, A.W. Partin, P. Kulkarni, R.H. Getzenberg, Cyr61 is regulated by cAMP-dependent protein kinase with serum levels correlating with prostate cancer aggressiveness, Prostate 72 (2012) 966–976.
[46] K. Prakash, G. Pirozzi, M. Elashoff, W. Munger, I. Waga, R. Dhir, Y. Kakehi, R.H. Getzenberg, Symptomatic and asymptomatic benign prostatic hyperplasia: molecular differentiation by using microarrays, Proc. Natl. Acad. Sci. U. S. A. 99 (2002) 7598–7603.
[47] V.N. Uversky, Natively unfolded proteins: a point where biology waits for physics, Protein Sci. 11 (2002) 739–756.

[48] A. Graneli, C.C. Yeykal, T.K. Prasad, E.C. Greene, Organized arrays of individual DNA molecules tethered to supported lipid bilayers, Langmuir 22 (2006) 292–299.

[49] E. Boukobza, A. Sonnenfeld, G. Haran, Immobilization in surface-tethered lipid vesicles as a new tool for single biomolecule spectroscopy, J. Phys. Chem. B 105 (2001) 12165–12170.

[50] U.B. Choi, P. Strop, M. Vrljic, S. Chu, A.T. Brunger, K.R. Weninger, Single-molecule FRET-derived model of the synaptotagmin 1-SNARE fusion complex, Nat. Struct. Mol. Biol. 17 (2010) 318–324.

[51] A.I.U. Grosberg, A.R. Khokhlov, Statistical Physics of Macromolecules, AIP Press, New York, 1994.

[52] P.J. Flory, Statistical Mechanics of Chain Molecules, Interscience Publishers, New York, 1969.

[53] D.K. Wilkins, S.B. Grimshaw, V. Receveur, C.M. Dobson, J.A. Jones, L.J. Smith, Hydro-dynamic radii of native and denatured proteins measured by pulse field gradient NMR techniques, Biochemistry 38 (1999) 16424–16431.

[54] C. Huang, Y. Wang, D. Li, Y. Li, J. Luo, W. Yuan, Y. Ou, C. Zhu, Y. Zhang, Z. Wang, M. Liu, X. Wu, Inhibition of transcriptional activities of AP-1 and c-Jun by a new zinc finger protein ZNF394, Biochem. Biophys. Res. Commun. 320 (2004) 1298–1305.

[55] A. Minden, A. Lin, M. McMahon, C. Lange-Carter, B. Derijard, R.J. Davis, G.L. Johnson, M. Karin, Differential activation of ERK and JNK mitogen-activated protein kinases by Raf-1 and MEKK, Science 266 (1994) 1719–1723.

[56] A. Lin, A. Minden, H. Martinetto, F.X. Claret, C. Lange-Carter, F. Mercurio, G.L. Johnson, M. Karin, Identification of a dual specificity kinase that activates the Jun kinases and p 38–Mpk2, Science 268 (1995) 286–290.

[57] R. Alani, P. Brown, B. Binetruy, H. Dosaka, R.K. Rosenberg, P. Angel, M. Karin, M.J. Birrer, The transactivating domain of the c-Jun proto-oncoprotein is required for cotransformation of rat embryo cells, Mol. Cell. Biol. 11 (1991) 6286–6295.

[58] I.G. Zigoneanu, Y.J. Yang, A.S. Krois, E. Haque, G.J. Pielak, Interaction of alpha-synuclein with vesicles that mimic mitochondrial membranes, Biochim. Biophys. Acta 1818 (2012) 512–519.

[59] M. Garofalo, G. Di Leva, G. Romano, G. Nuovo, S.S. Suh, A. Ngankeu, C. Taccioli, F. Pichiorri, H. Alder, P. Secchiero, P. Gasparini, A. Gonelli, S. Costinean, M. Acunzo, G. Condorelli, C.M. Croce, miR-221&222 regulate TRAIL resistance and enhance tumorigenicity through PTEN and TIMP3 downregulation, Cancer Cell 16 (2009) 498–509.

[60] P. Pineau, S. Volinia, K. McJunkin, A. Marchio, C. Battiston, B. Terris, V. Mazzaferro, S.W. Lowe, C.M. Croce, A. Dejean, miR-221 overexpression contributes to liver tumorigenesis, Proc. Natl. Acad. Sci. U. S. A. 107 (2010) 264–269.

[61] S. Galardi, N. Mercatelli, M.G. Farace, S.A. Ciafre, NF-kB and c-Jun induce the expression of the oncogenic miR-221 and miR-222 in prostate carcinoma and glioblastoma cells, Nucleic Acids Res. 39 (2011) 3892–3902.

[62] N. Sato, M.D. Sadar, N. Bruchovsky, F. Saatcioglu, P.S. Rennie, S. Sato, P.H. Lange, M.E. Gleave, Androgenic induction of prostate-specific antigen gene is repressed by protein-protein interaction between the androgen receptor and AP-1/c-Jun in the human prostate cancer cell line LNCaP, J. Biol. Chem. 272 (1997) 17485–17494.

[63] S.Y. Chen, C. Cai, C.J. Fisher, Z. Zheng, J. Omwancha, C.L. Hsieh, L. Shemshedini, c-Jun enhancement of androgen receptor transactivation is associated with prostate cancer cell proliferation, Oncogene 25 (2006) 7212–7223.

[64] C. Cai, C.L. Hsieh, L. Shemshedini, c-Jun has multiple enhancing activities in the novel cross talk between the androgen receptor and Ets variant gene 1 in prostate cancer, Mol. Cancer Res. 5 (2007) 725–735.

[65] W. Li, C.L. Wu, P.G. Febbo, A.F. Olumi, Stromally expressed c-Jun regulates proliferation of prostate epithelial cells, Am. J. Pathol. 171 (2007) 1189–1198.

[66] J. Edwards, N.S. Krishna, R. Mukherjee, J.M. Bartlett, The role of c-Jun and c-Fos expression in androgen-independent prostate cancer, J. Pathol. 204 (2004) 153–158.

[67] T. Sun, M. Yang, S. Chen, S. Balk, M. Pomerantz, C.L. Hsieh, M. Brown, G.S. Lee, P.W. Kantoff, The altered expression of MiR-221/-222 and MiR-23b/-27b is associated with the development of human castration resistant prostate cancer, Prostate 72 (2012) 1093–1103.

[68] X. Ouyang, W.J. Jessen, H. Al-Ahmadie, A.M. Serio, Y. Lin, W.J. Shih, V.E. Reuter, P.T. Scardino, M.M. Shen, B.J. Aronow, A.J. Vickers, W.L. Gerald, C. Abate-Shen, Activator protein-1 transcription factors are associated with progression and recurrence of prostate cancer, Cancer Res. 68 (2008) 2132–2144.

[69] M. Karin, Z. Liu, E. Zandi, AP-1 function and regulation, Curr. Opin. Cell Biol. 9 (1997) 240–246.

[70] L. Ciapponi, D. Bohmann, An essential function of AP-1 heterodimers in Drosophila development, Mech. Dev. 115 (2002) 35–40.